Intrinsic n-type Defect Formation in TiO_2: A Comparison of Rutile and Anatase from GGA+*U* Calculations

Benjamin J. Morgan* and Graeme W. Watson*

School of Chemistry, Trinity College Dublin, Dublin 2, Ireland

Received: September 11, 2009; Revised Manuscript Received: November 27, 2009

The formations of intrinsic n-type defects, that is, oxygen vacancies and titanium interstitials, in rutile and anatase TiO_2 have been compared using GGA+*U* calculations. In both crystal structures, these defects give rise to states in the band gap, corresponding to electrons localized at Ti^{3+} centers. O vacancy formation in rutile results in two excess electrons occupying 3d orbitals on Ti atoms neighboring the vacancy. Similarly, for anatase, two Ti 3d orbitals are occupied by the excess electrons, with one of these Ti sites neighboring the vacancy, and the second at a next-nearest Ti position. This localization is accompanied by one oxygen moving toward the vacancy site to give a "split vacancy" geometry. A second fully localized solution is also found for anatase, with both occupied Ti sites neighboring the vacancy site. This minimum is 0.05 eV less stable than the split vacancy and is thus expected to be present in experimental samples. A partially delocalized solution corresponding to the split vacancy geometry, with one electron occupying the bottom of the conduction band, is also identified as 0.28 eV less stable. Formation of titanium interstitials donates four electrons to the Ti lattice. In anatase, one of these electrons is located at the interstitial Ti site, and three occupied defect states are hybridized between three nearest neighbor Ti sites. In rutile, these excess electrons are mostly localized at four nearest neighbor Ti sites, with only a small amount of excess charge found on the interstitial Ti atom. This difference in the charge on the interstitial atom is a consequence of the differing interstitial geometries in the two polymorphs. Calculated optical absorption spectra for all defects show significant decreases of the optical band gap, with a larger red shift predicted for titanium interstitials in anatase than in rutile. Defect formation energies have been calculated under oxygen-rich and oxygen-poor conditions for both polymorphs. Under all conditions, O vacancy formation is slightly more favorable in anatase than in rutile, while Ti interstitials form more easily in rutile than anatase. Under O-rich conditions, O vacancies are the favored defect type, but both defect types have high formation energies. Under O-poor conditions, both defect types are stabilized, with Ti interstitials predicted to become the favored defect in rutile samples, particularly at elevated temperatures.

I. Introduction

TiO_2 has numerous applications including photocatalysis,[1] water splitting,[2] and solar cell technologies[3] and is also widely studied as a model metal oxide. These technological uses involve photogeneration of electron−hole pairs, which then diffuse through the crystal to reactant molecules absorbed at the surface or to electrodes. Under standard conditions, TiO_2 is substoichiometric with a titanium excess. This substoichiometry can be accommodated as oxygen vacancies, V_O, or titanium interstitials, Ti_i. Both of these defect species are likely to be present in typical samples, with competition between defect types determined by synthesis conditions and sample history.

TiO_2 most commonly crystallizes in either the rutile (space group $P4_2/mnm$) or the anatase (space group I_1/amd) phase. Both are constructed from distorted TiO_6 octahedra, with the relative arrangement of these determining the overall structure. Rutile is more easily formed as single crystals, and as such has been the subject of the majority of previous research. Anatase, however, demonstrates improved photocatalytic activity as compared to rutile, and thus is the preferred polymorph for many applications. The reasons for this contrast in physical properties are yet to be determined, and it is possible that differences in defect behavior play a role.[4] Differing crystal structures mean defects are expected to form at different concentrations in rutile and anatase. The effect of otherwise equivalent defects on photocatalytic properties may also differ between the two polymorphs.

Reduced TiO_2 is experimentally characterized by the presence of defect states that are visible in the band gap in photoelectron spectra.[5−8] These band gap states have been assigned to Ti^{3+} species on the basis of EPR data[9,10] and Ti core-level shifts.[11] The presence of defects thus alters the electronic structure of the system, with consequences for photoelectronic behavior; gap states effectively narrow the optical band gap, allowing optical absorption within the visible spectrum, and giving rise to the characteristic blue color of reduced samples.[12,13] Although increased visible light absorption can lead to improved photocatalytic behavior, defect sites can impair quantum yields by acting as recombination centers for photogenerated electron−hole pairs.[14]

In both anatase and rutile TiO_2, the conduction band is predominantly made up from Ti 3d states, which are formally unoccupied in the stoichiometric material. These Ti valence states are highly localized, and the formation of intrinsic n-type defects donates electrons to the Ti lattice. These occupy Ti 3d conduction band states to produce the localized defect states observed experimentally. Standard DFT functionals fail to

* To whom correspondence should be addressed. E-mail: morganb@tcd.ie (B.J.M.); watsong@tcd.ie (G.W.W.).

10.1021/jp9088047
Published on Web 01/15/2010

provide even a qualitatively correct description of such behavior due to the self-interaction error.[15,16] This results in occupation of the bottom of the conduction band, to give a metallic description associated with delocalization of the excess charge over multiple Ti centers.[17−19] The frequent failure of standard density functional theory (DFT) functionals to describe the partial occupation of states characterized by highly localized orbitals is well documented, having been demonstrated in a number of transition metal and rare earth oxides.[20−24]

The use of hybrid functionals, where a proportion of Hartree−Fock exchange is mixed into the DFT functional, and use of DFT+U techniques, where the on-site Coulomb interaction for the localized states of interest is explicitly described within a Hubbard-like framework, have both been successful in correcting for the delocalization bias of standard DFT functionals. These methods have been applied to TiO_2 to recover descriptions that are in good agreement with experimental data for both intrinsic[18,25−28] and extrinsic n-type defects.[28−30]

Oxygen vacancies in rutile have been studied using hybrid DFT by Islam et al. who found the excess charge was mostly present at the three titanium sites next to the O vacancy.[31] The rutile O vacancy was also modeled using DFT+U by Mattioli et al. who reported a fully localized description with only two of the near-vacancy Ti 3d orbitals occupied,[4] suggesting the hybrid functional used by Islam et al. (PW1PW: 20% HF-exchange) had insufficient exact exchange to correct the DFT self-interaction error.

Mattioli et al. also used DFT+U to model oxygen vacancies in anatase, where they reported a partially delocalized solution, with one electron occupying a Ti 3d orbital in a site adjacent to the vacancy, and the second occupying the bottom of the conduction band and delocalized over all of the Ti sites in the calculation.[4] O vacancies in anatase TiO_2 have also been modeled by Finazzi et al. using standard GGA, GGA+U, and hybrid DFT methods.[18] The use of GGA+U and hybrid DFT enables localized solutions to be obtained, with the degree of localization dependent on the value of U or proportion of Hartree−Fock exchange included in the functional. Full localization of both electrons was only achieved with sufficiently large corrections to the self-interaction error ($U \geq 3.0$ eV for GGA+U, and 50% HF-exchange within the H&HLYP hybrid functional).

Finazzi et al. have also considered Ti interstitial formation in both rutile and anatase TiO_2 using hybrid DFT.[32] For anatase, they reported one electron localized at the interstitial Ti atom, and three electrons partially localized on surrounding Ti sites. For rutile, more complete localization of the excess charge was reported, again with one electron on the interstitial Ti, and the remaining three electrons on coordinated lattice Ti sites.

Although oxygen vacancies and titanium interstitials have been previously modeled in both anatase and rutile, to date there has been no single study that considered both defect types in both TiO_2 polymorphs. A direct comparison of defect properties, in particular formation energies and hence defect concentrations, is therefore problematic. In this Article, we report calculations of oxygen vacancies, V_O, and titanium interstitials, Ti_i, in rutile and anatase TiO_2 using GGA+U. By considering all four defect types with a consistent theoretical method, we are able to compare electronic structures between polymorphs, and to calculate consistent optical absorption spectra and defect formation energies across the full range of accessible chemical potentials.

II. Theoretical Methods

All calculations were performed using the density functional theory (DFT) code VASP,[33,34] in which valence electronic states are expanded with a plane-wave basis set, with an energy cutoff of 500 eV. The Perdew−Berke−Ernzerhof (PBE) GGA exchange-correlation functional[35] was supplemented by the Dudarev +U correction[36] to allow the strongly correlated nature of the occupied Ti 3d states to be correctly described. A value of $U_{Ti}(d) = 4.2$ eV was used, which has previously been shown to reproduce the experimentally observed position of the defect state of O vacancies at the rutile (110) surface.[26,37] Valence−core interactions were described with the projector-augmented wave approach,[38,39] with cores of [Ar] for Ti and [He] for O. Real space projection was used for the PAW operators, with the projection operators optimized to an accuracy of 1.0×10^{-4} eV Å^{-1}, and sufficient G vectors included in the Fourier transformations that wrap-around errors were avoided.

To obtain optimized lattice parameters, constant volume calculations of stoichiometric unit cells (6 atoms for rutile, 12 atoms for anatase) with $4 \times 4 \times 6$ (rutile) or $6 \times 6 \times 2$ (anatase) Monkhorst−Pack k-point meshes were performed at a series of volumes, and the resultant energy−volume data were fitted to the Murnaghan equation of state. This approach eliminates the problem of Pulay stress that occurs when cell volumes are allowed to fluctuate in plane-wave calculations. This gave optimized lattice parameters of $a = 4.700$ Å and $c = 3.043$ Å for rutile, and $a = 3.907$ Å and $c = 9.724$ Å for anatase.

The defect calculations were performed using a $3 \times 3 \times 1$ supercell for anatase (108 atoms), and a $3 \times 3 \times 4$ supercell for rutile (216 atoms), both with $2 \times 2 \times 2$ Monkhorst−Pack k-point sampling. All calculations were spin polarized and were geometrically optimized without symmetry or spin constraints, with structures deemed to be converged when the forces on all atoms were less than 0.01 eV Å^{-1}.

III. Results

A. Electronic Structure. ***1. O Vacancies.*** In both rutile and anatase, oxygen vacancy formation produces a new feature in the band gap of the electronic density of states (EDOS), Figure 1: (a) rutile and (b) anatase. For rutile, this feature is a double peak and is offset from the conduction band minimum (CBM) by 1.6 eV. The projected charge density associated with this defect state is strongly localized on two Ti atoms neighboring the vacancy site, with small contributions from adjacent O 2p states, Figure 2. The double peak of the EDOS gap state feature is due to the interaction of these two occupied Ti 3d orbitals, as seen in previous studies.[4,26,29] The O vacancy in anatase produces a single gap-state peak 1.5 eV below the CBM, which also corresponds to strong localization at two Ti atoms. Here though, only one of these occupied Ti sites is in a position adjacent to the vacancy. The second is at a next-nearest Ti site in the mutual (100) plane. One oxygen initially coordinated to the next-nearest Ti site moves away from this position and toward the vacancy site to give a "split vacancy" geometry, in agreement with the hybrid DFT calculations of Finazzi et al.[18] (geometries and interatomic distances are shown in Figures S1−4). For both rutile and anatase, the accommodation of the excess charge in two strongly localized Ti 3d orbitals allows vacancy formation to be formally described as $O_O^{\times} + 2Ti_{Ti}^{\times} \rightarrow V_O^{\bullet\bullet} + 2Ti_{Ti}'$. Projecting the defect state charge densities onto atom-centered spherical harmonics of radii 1.37 Å (cf. ref 26) gives 3d occupations of 0.71 and 0.71 e for the Ti centers neighboring the vacancy in rutile, 0.69 (neighboring) and 0.65 e

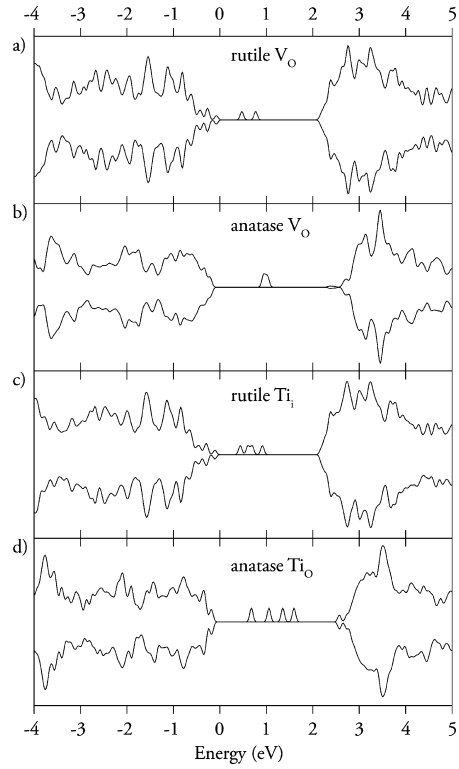

Figure 1. Electronic density of states (EDOS) for oxygen vacancies and titanium interstitials in TiO_2: (a) V_O in rutile, (b) V_O in anatase, (c) Ti_i in rutile, and (d) Ti_i in anatase.

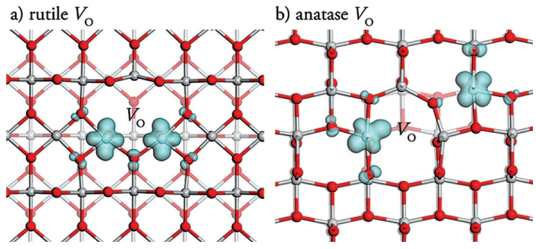

Figure 2. Partial charge densities for the oxygen vacancy defect states in (a) rutile and (b) anatase TiO_2. In each case, the charge densities correspond to the defect states in Figure 1a and b. The isosurfaces are shown at 0.05 e $Å^{-3}$.

(next-nearest neighbor) for the split vacancy in anatase. All other Ti centers showed occupancies below 0.05 e.

A second fully localized oxygen vacancy solution for anatase was also observed. In this case, the two occupied Ti 3d orbitals are both at Ti sites neighboring the vacancy, Figure 3a, giving an electronic structure similar to that seen for V_O in rutile. The "simple vacancy" solution found here is predicted to be 0.05 eV higher in energy than the split vacancy described above. Because these two localized vacancy solutions are very close in energy, it is interesting to consider the effect of varying the U parameter on their relative stabilities. Further optimization of the simple and split vacancies with an unphysically large value of U of 7 eV resulted in stable geometries with the simple vacancy configuration now more stable than the split vacancy by 57 meV. Hence, the relative energies of the two solutions show only weak dependence on the value of U. Because the energy differences are small, however, we are not able to unambiguously determine the most stable vacancy structure, and both simple and split geometries are expected to be present in experimental samples. However, our results suggest that for physically reasonable values of U there is a small preference

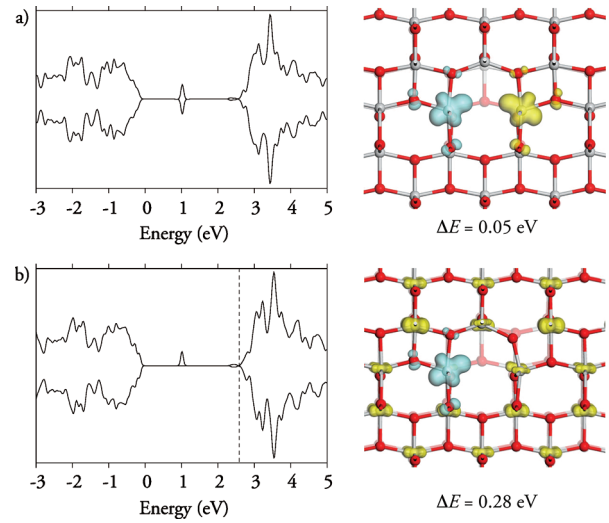

Figure 3. Electronic densities of states (EDOS) and partial charges for the metastable oxygen vacancy defect states in anatase TiO_2. (a) The fully localized "simple vacancy". The partial charge density for the defect state peaks is shown at an isosurface of 0.05 e $Å^{-3}$. The blue and yellow isosurfaces show the partial charges for the α and β spin components of the defect state. (b) The partially localized "split vacancy". Only one gap state is seen in the EDOS, and the bottom of the conduction band is occupied. The vertical dashed line shows the Fermi level. The partial charge densities are shown for the gap state in blue at an isosurface of 0.05 e $Å^{-3}$, and for the occupied conduction band states in yellow at 0.02 e $Å^{-3}$. ΔE gives the energy of each defect configuration relative to the localized "split" vacancy.

for the split vacancy geometry. Projected charge densities for the defect states give 3d occupancies of 2 × 0.64 e for the Ti atoms neighboring the vacancy.

By distorting the starting geometry and setting initial magnetic moments on the Ti atoms, a partially delocalized solution with the split vacancy geometry was obtained, Figure 3b. Only one electron is localized at a vacancy-neighboring Ti site, giving rise to a band gap defect peak, whereas the second electron is delocalized over all of the Ti atoms in the calculation, and occupies the bottom of the conduction band. Mattioli et al. have reported a partially delocalized DFT+U solution for V_O in anatase and suggested that such electronic states explain the improved electron transport in anatase relative to rutile.[4] Similar partially delocalized solutions for anatase were also predicted by Finazzi et al.[18] with both GGA+U (U = 3 eV) and hybrid DFT (B3LYP, α = 25%). For both methods, however, fully localized solutions with both electrons occupying single Ti 3d orbitals were also obtained, which in each case were more stable than the partially delocalized solution (ΔE = 0.07 eV for GGA+U, U = 3 eV, and 0.06 eV for B3LYP). Finazzi et al. further reported that for both calculation methods, with larger self-interaction error corrections applied (U = 4 eV and α = 50%), only fully localized solutions were predicted. This is due to larger self-interaction corrections acting to remove more of the delocalization bias of the standard DFT functional. The partially delocalized solution reported here is 0.28 eV less stable than the fully localized split vacancy. It should be noted, however, that the relative energies of fully localized versus partially (or fully) delocalized solutions will be sensitive to the degree of self-interaction correction used in specific calculations, making it difficult to directly compare the energy differences for these alternate solutions obtained with different methods. Furthermore, it can be misleading to directly compare energies for localized and delocalized defect states using k-point sampling chosen to give converged energies for the bulk material, because

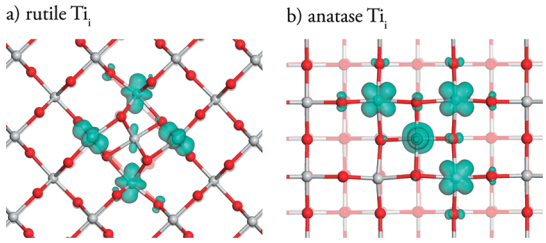

Figure 4. Partial charge densities for the titanium interstitial defect states in (a) rutile and (b) anatase TiO_2. The isosurfaces are shown at 0.05 e Å^{-3}. Both images are viewed along the [001] crystal axes.

this is likely to be grossly insufficient for accurate energies of delocalized solutions where the band edges are occupied.

Yang et al. have recently reported GGA+U calculations in which strong preference for singlet over triplet alignment of the spins at the Ti^{3+} centers was predicted for both rutile and anatase.[40] The energy difference between singlet and triplet spin states was reported to be 0.47 eV for anatase and 0.18 eV for rutile. This is in contrast with the previous calculations by Finazzi et al.[18] and Mattioli et al.[4] for which fully localized solutions were reported to have triplet spin configurations. We performed calculations for the rutile oxygen vacancy, and the anatase split and simple oxygen vacancies, with the total spin constrained to both 0 and 2 μB. In all cases, the differences between singlet and triplet spin solutions were negligible. For the rutile oxygen vacancy, the triplet solution is favored by 5 meV, and for the anatase split vacancy the difference in energy between singlet and triplet solutions is less than 1 meV. The anatase simple vacancy showed a preference for the singlet solution by 23 meV. This mirrors calculations performed on CeO_2, for which formation of oxygen vacancies also results in the localization of two excess electrons at nearby metal centers with little preference between relative spin orientations.[41,42]

2. Ti Interstitials. The electronic densities of states for titanium interstitials also show new gap states for both rutile, Figure 1c, and anatase, Figure 1d. For both polymorphs, these Ti_i defect states correspond to four electrons. In contrast to O vacancies, there are significant differences in the distribution of the electronic states; the four defect peaks are more widely dispersed along the energy scale for anatase (0.91 eV) than for rutile (0.47 eV). These states appear lower in the gap for rutile than anatase, as for the O vacancies, but this is in part due to the larger band gap of anatase. The conduction band offsets of the peaks are in the range 1.74−1.26 eV for rutile and 1.84−0.98 eV for anatase.

The partial charge distributions associated with these defect states are shown in Figure 4. For rutile, panel (a), the interstitial site lies at the center of an oxygen octahedron, with six nearest-neighbor Ti atoms. Two of these are in the same [001] plane as the interstitial atom, and can be considered as axial neighboring Ti-sites, with the remainder paired in front and behind this [001] plane, providing four equatorial neighboring sites. The majority of the excess charge is localized in 3d orbitals on four of the nearest neighbor Ti sites: the two axial Ti sites, and two of the equatorial Ti sites sharing a common [001] plane. The occupied orbitals on the equatorial sites have d_{xy}-like character, with lobes oriented between Ti−O bonds, and the occupied orbitals on the axial sites have d_{z^2}-like character, again with lobes oriented away from local Ti−O bonds, and with one lobe oriented toward the interstitial Ti site. This orientation allows some of the excess charge to delocalize on the interstitial site. Projecting defect state charge densities onto spherical harmonics of radii 1.37 Å gives Ti 3d occupancies of 0.12e for Ti_i, 2 × 0.55 e for axial Ti_{Ti}, and 2 × 0.73 e for equatorial Ti_{Ti}.

The partial charges associated with each of the four occupied Kohn−Sham orbitals that contribute to the defect state are shown in Figure 5. Each peak has contributions from two or more of the occupied Ti 3d orbitals, indicating significant orbital−orbital interactions. The lowest energy gap state has some charge associated with the interstitial Ti site, whereas the higher energy gap states are more strongly localized on only the Ti sites that make up the coordination octahedron. This shows some agreement with the previous work of Finazzi et al. who reported that charge fully localized at the Ti int site is responsible for the deepest gap states.[32]

The interstitial site in anatase also has a nearest-neighbor oxygen coordination that is a distorted octahedron (D_{2d} symmetry), with four adjacent lattice Ti sites as the closest cation neighbors. The excess charge is strongly localized at the interstitial atom, in a $3d_{z^2}$ orbital, and at three of the neighboring Ti sites, where it is accommodated in $3d_{xy}$ orbitals, Figure 4b. As for the rutile Ti interstitial, there is a small amount of charge found on neighboring O 2p sites. The spherical harmonic projected charge densities are 0.74 e for Ti_i and 3 × 0.66 e for the occupied Ti_{Ti}. The partial charges of each of the four Kohn−Sham orbitals that make up the defect states are shown in Figure 6. Here, the lowest occupied state is solely associated with the occupied $3d_{z^2}$ orbital on the interstitial Ti atom, whereas the remaining three occupied states each has contributions from more than one of the occupied $3d_{xy}$ orbitals, again indicating orbital−orbital interactions. The preferential occupation of the $3d_{z^2}$ orbital for the interstitial atom is due to the crystal field effects of the [4 + 2] distorted octahedral coordination; in the stoichiometric system, the Ti−O distances are 1.99 Å for equatorial bonds and 2.02 Å for axial bonds. For the interstitial site, the equivalent distances are 1.96 and 2.85 Å, significantly stabilizing the $3d_{z^2}$ orbital (detailed interatomic distances for the titanium interstitial in rutile and anatase are shown in Figures S6 and S7). If the interstitial $3d_{z^2}$ peak is ignored, the splitting in energy of gap state features is similar for rutile and anatase.

B. Optical Absorption Spectra. Reduced TiO_2 demonstrates enhanced photocatalytic activity for several processes, including the degradation of environmental pollutants[43] and solar energy conversion.[3,44] Improved solar efficiencies are attributed to the presence of defect states in the band gap enabling photoexcitation from the absorption of visible light. To examine the effect of defects on absorption profiles, we have calculated absorption spectra for each of the defect systems in both rutile and anatase, and those of the stoichiometric systems for comparison.

Optical absorption spectra were calculated using the transversal approximation and PAW approach.[45] The optical matrix elements, $\hat{P}_\alpha^{fi} = \langle \Psi_f | \hat{P}_\alpha | \Psi_i \rangle$, where $\hat{P}_\alpha$ is the momentum operator with polarization α, and Ψ are PAW all-electron wave functions, are calculated using the method of Adolph et al.[46] The imaginary part of the dielectric function is given by

$$\mathrm{Im}\ \varepsilon_{\alpha\beta}(\omega) = \left(\frac{2\pi e}{m\omega}\right)^2 \sum_{if} \int \hat{P}_\alpha^{if} \hat{P}_\beta^{fi} \delta[E_f(\mathbf{k}) - E_i(\mathbf{k}) - \hbar\omega]\, \mathrm{d}(\mathbf{k}) \quad (1)$$

with the integration performed using the tetrahedron method[38] and a fine Γ-centered (4 × 4 × 4) Monkhorst−Pack k-point mesh. The real part of the dielectric function, Re $\varepsilon_{\alpha\beta}(\omega)$, can be obtained

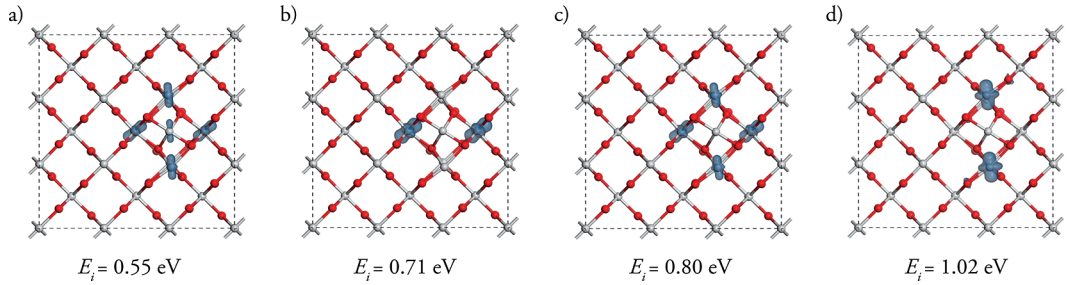

Figure 5. Partial charge densities for the defect states of a Ti interstitial in rutile TiO_2. Panels (a)−(d) correspond to the gap state peaks in Figure 1c. The isosurfaces are shown at 0.05 e $Å^{-3}$, and the energies, E_i, are relative to the valence band maximum.

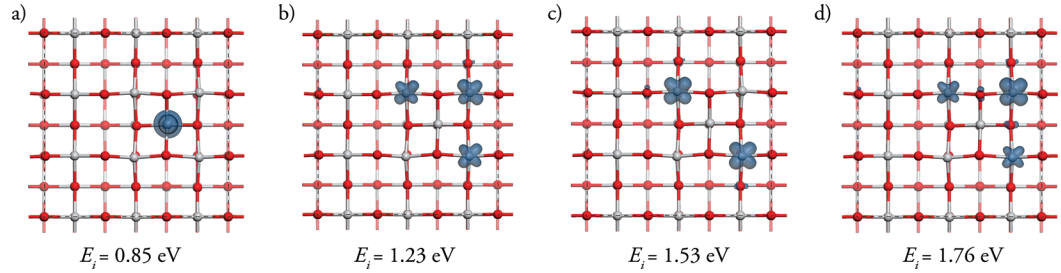

Figure 6. Partial charge densities for the defect states of a Ti interstitial in anatase TiO_2. Panels (a)−(d) correspond to the gap state peaks in Figure 1d. The isosurfaces are shown at 0.05 e $Å^{-3}$, and the energies, E_i, are relative to the valence band maximum.

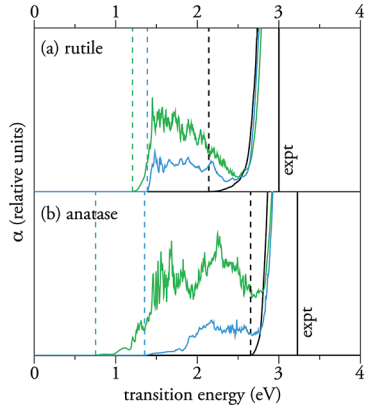

Figure 7. Calculated optical absorption spectra for (a) rutile and (b) anatase TiO_2. For each structure, the spectrum for the stoichiometric system is black, and the spectra for Ti_i and V_O are green and blue, respectively. The dashed vertical lines give the onset of absorption, that is, the minimum energy for which $\alpha \neq 0$. The solid vertical lines are the optical band gaps of 3.0 and 3.2 eV from experiment.[50]

from Im $\varepsilon_{\alpha\beta}(\omega)$ using the Kramers−Kronig relations.[47] The absorption coefficient is given by

$$\alpha(\omega) = \frac{\sqrt{2[|\varepsilon_{\alpha\alpha}(\omega)| - \mathrm{Re}\ \varepsilon_{\alpha\alpha}(\omega)]}}{c} \qquad (2)$$

The absorption spectra are summed over all direct transitions between occupied and unoccupied Kohn−Sham orbitals, and therefore ignores indirect and intraband absorptions.[46] Within this framework of single particle transitions, the electron−hole correlations are not treated and would require treatment by higher order electronic structure methods.[48,49]

The calculated absorption spectra are shown in Figure 7. For the stoichiometric systems, both rutile and anatase have predicted absorption onsets below the experimentally observed band gaps of 3.0 and 3.2 eV,[50] due to the underestimation of the fundamental gap common to GGA calculations, which is only partially corrected by the addition of the Dudarev $+U$. For both crystal structures, the introduction of both defect types produces weak absorption at energies red-shifted relative to the absorption onset in the stoichiometric materials. This shift is larger for titanium interstitials than oxygen vacancies, and for Ti interstitials the red shift is larger in anatase than in rutile. These differences are a consequence of the defect peak positions seen in Figure 1, specifically the Ti d−d splitting between the highest occupied defect state and the conduction band minimum. For both rutile and anatase, the defect states are lower in the band gap for V_O than for Ti_i, and for titanium interstitials, the conduction band offset of the highest occupied defect state is smaller in anatase than in rutile.

C. Formation Energies. Defect formation energies, $\Delta H_f(D)$, are calculated according to

$$\Delta H_f(D) = E_{TiO_2[D]} - E_{TiO_2} + n_{Ti}\mu_{Ti} + n_O\mu_O \qquad (3)$$

where E_{TiO_2} and $E_{TiO_2[D]}$, respectively, are the calculated energies of the stoichiometric and defective supercells, and n_{Ti} and n_O are the numbers of Ti and O atoms transferred from reservoirs with respective chemical potentials μ_{Ti} and μ_O. These chemical potentials are with respect to GGA$+U$ calculated reference energies for the elements in their standard states, that is, $Ti_{(s)}$ and $O_{2(g)}$.[51] For TiO_2 under equilibrium conditions, these chemical potentials are such that

$$\mu_{Ti} + 2\mu_O = \Delta H_f(TiO_2) \qquad (4)$$

which is calculated to be −8.87 eV for anatase and −8.91 eV for rutile. Further limits are placed on the allowed variation in chemical potentials, because TiO_2 is required to be thermodynamically stable with respect to formation of Ti_2O_3, that is:

$$2\mu_{Ti} + 3\mu_O \leq \Delta H_f(Ti_2O_3) \qquad (5)$$

which is calculated to be −14.20 eV. Under O-rich conditions, the system is in equilibrium with $O_{2(g)}$, fixing μ_O as 0 eV. Under

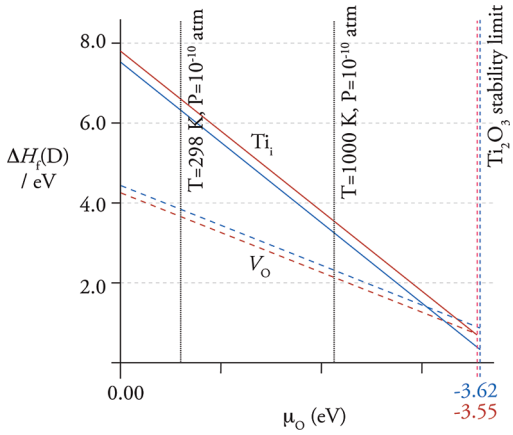

Figure 8. Formation energies for oxygen vacancies (V_O) and titanium interstitials (Ti_i) in rutile (blue) and anatase (red), as a function of oxygen chemical potentials, μ_O. The vertical lines to the right of the plot show the $TiO_2 \rightarrow Ti_2O_3$ stability limit for rutile at 3.62 eV and anatase at 3.55 eV. The vertical dotted lines give μ_O at $T = 298$ K, $p = 10^{-10}$ atm, and $T = 1000$ K, $p = 10^{-10}$ atm.

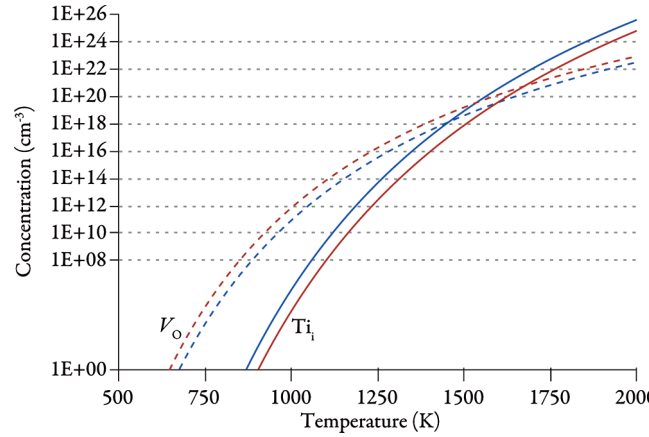

Figure 9. Temperature dependence of defect concentrations for O vacancies (dashed) and Ti interstitials (solid) in rutile (blue) and anatase (red) TiO_2 for $P = 10^{-10}$ atm.

limiting O-poor/Ti-rich conditions, the phase boundary with Ti_2O_3 occurs where $\Delta H_f(TiO_2) = \Delta H_f(Ti_2O_3)$, and the constituent chemical potentials are obtained by solving the resultant pair of simultaneous equations. For anatase, these requirements give bounding end-points of $\mu_O = 0$ eV, $\mu_{Ti} = -8.87$ eV for oxygen-rich conditions, and $\mu_O = -3.55$ eV, $\mu_{Ti} = -1.78$ eV for titanium-rich conditions; and for rutile the bounding end-points are $\mu_O = 0$ eV, $\mu_{Ti} = 8.91$ eV for oxygen-rich conditions, and $\mu_O = -3.62$ eV, $\mu_{Ti} = -1.67$ eV for titanium-rich conditions.

The variation in defect formation energies across these ranges of chemical potentials is shown in Figure 8. The general trends for rutile and anatase are similar: under O-rich conditions, O vacancies are the favored defect, with formation energies of 4.41 eV for rutile and 4.23 eV for anatase, whereas Ti interstitials have formation energies of 7.50 and 7.74 eV. Under limiting Ti-rich conditions, both defect types are predicted to form more readily with defect formation energies for O vacancies of 0.80 and 0.70 eV, and for Ti interstitials of 0.26 and 0.70 eV.

The effect of temperature and pressure on the defect formation energies can be approximated by considering the enthalpic and entropic contributions to the oxygen chemical potential μ_O in the O_2 gas phase. The direct effects of temperature and pressure on μ_{Ti}, $\Delta H_f(TiO_2)$, and $\Delta H_f(Ti_2O_3)$ are neglected as these are either small ($P\Delta V$ terms) or expected to largely cancel ($T\Delta S_{vib}$ terms); μ_{Ti} is affected through the constraint $\mu_{Ti} + 2\mu_O = \Delta H_f(TiO_2)$. Using the experimental value for the $O_{2(g)}$ standard entropy, $S_0 = 205$ J mol^{-1} K^{-1},[52] the change in μ_O can be expressed as:[53]

$$\Delta\mu_O(T,P) = \frac{1}{2}\left\{[C_P(T - T_0)] - T\left[S_0 + C_P \ln\frac{T}{T_0} + k_B T \ln\frac{P}{P_0}\right]\right\} \quad (6)$$

Using the ideal gas law, we use $C_P = (7/2)k_B$ for the constant-pressure specific heat capacity per diatomic molecule, which reproduces well the experimentally tabulated $\Delta\mu_O(T, P)$.[54] In general, increasing temperature and decreasing $p(O_2)$ result in decreasing μ_O. The vertical dotted lines in figure 8 show example calculated values of μ_O for $T = 298$ K, $P = 10^{-10}$ atm, and $T = 1000$ K, $P = 10^{-10}$ atm. Having calculated the temperature dependence of the defect formation energies, defect concentrations as a function of temperature can be estimated assuming Arrhenius-type behavior. Figure 9 shows such defect concentrations between 500 and 2000 K for an oxygen partial pressure of 10^{-10} atm, which might be a typical vacuum pressure for the synthesis of O-poor samples. As the temperature is increased, concentrations of both oxygen vacancies and titanium interstitials increase, with the change being largest for Ti_i. This results in Ti interstitials becoming the dominant defect at elevated temperatures, in agreement with the defect behavior indicated by electrical conductivity measurements.[55]

IV. Summary and Discussion

Density functional theory implemented within GGA+U has been used to compare oxygen vacancies and titanium interstitials in rutile and anatase TiO_2. In rutile, oxygen vacancy formation results in two electrons donated to the crystal lattice occupying 3d orbitals at Ti sites adjacent to the vacancy. This solution is congruous with recent EPR data that were interpreted as showing electrons trapped at two Ti sites neighboring the vacancy and aligned in the [001] direction.[10] For oxygen vacancies in anatase, a "split" geometry is favored, as seen in previous hybrid DFT calculations.[18] One O atom coordinated to a vacancy-neighboring Ti moves partially toward the vacancy site, and the excess charge localizes at the second vacancy-neighboring Ti and one Ti site initially coordinated to the displaced oxygen. A second fully localized "simple vacancy" solution, with both electrons accommodated at Ti sites neighboring the vacancy, is also observed and is 0.05 eV less stable than the localized split vacancy. Electron transport in TiO_2 occurs via hopping of localized small polarons,[56] and different possible positions of these polarons result in a complex potential energy landscape with many local minima,[57] as has been reported for other partially reduced oxides where the valence band states are strongly localized.[58,59] While the detailed study of the configuration space of such polarons and their interactions with atomic defects is a hugely complex problem, the closeness in energy of both of the fully localized states reported here suggests that oxygen vacancies in anatase only weakly trap itinerant electrons. A third anatase O vacancy solution was also obtained, corresponding to the split vacancy geometry with only one electron trapped at a vacancy-neighboring Ti site, and the second electron occupying the bottom of the conduction band. This solution is 0.28 eV less favorable than the localized split vacancy.

For defects with occupied states above the valence band edge, the underestimation of the band gap inherent to LDA/GGA

methods can affect the defect formation energies.[60] For TiO_2, the defect states and conduction band states are largely formed from Ti 3d states, with some O 2p mixing. It is therefore expected that extrapolation of the band gap to the experimental values (3.0 eV for rutile and 3.2 eV for anatase[50]) would shift the conduction band edge and the localized Ti 3d defect states by equivalent values.[61] Thus, the relative energy of the three defect states would remain unchanged. Because the calculated differences between the split and simple vacancies are very small, however, small errors in such an extrapolation may affect the relative energy ordering, and we cannot conclusively identify which of the two fully localized defects is most stable,[62] although they are expected to both be present in experimental systems.

Titanium interstitials donate four electrons to the system. In rutile, the lowest energy solution obtained localizes the majority of charge at four of the Ti sites neighboring the interstitial site: two in axial and two in equatorial positions of the coordination octahedron, with a small portion of charge (0.12e) on the interstitial atom. The titanium interstitial in anatase conversely strongly localizes the excess charge at the interstitial atom and three of the neighboring Ti sites. The [4 + 2] pseudosquare planar coordination stabilizes the $3d_{z^2}$ orbital, making electron trapping at the interstitial site favorable. This is in contrast to the near-octahedral interstitial coordination achieved in rutile, which affords no significant crystal field stabilization of orbitals on the interstitial Ti. Formally, this difference in distribution of electronic charge can be expressed as $[Ti_i^{\bullet\bullet\bullet\bullet} + 4Ti'_{Ti}]$ for rutile and $[Ti_i^{\bullet\bullet\bullet} + 3Ti'_{Ti}]$ for anatase.

Both defect types produce a red shift in the onset of optical absorption in anatase and rutile, as is seen experimentally. The magnitude of reduction of the optical band gap is greater for anatase than for rutile, due to a smaller d−d splitting between occupied and unoccupied Ti 3d states.

Under O-rich conditions, concentrations of both intrinsic defects are expected to be low, with O vacancies greatly favored over Ti interstitials. Under O-poor conditions, both defect types are expected to form much more readily, and Ti interstitials become comparable in energy with O vacancies. Rutile, in particular, is stable within a region of low O chemical potential where Ti interstitials are expected to form more readily than O vacancies. Because defect sites are expected to act as recombination centers for photogenerated electron−hole pairs,[63] this increased tendency for Ti interstitial in rutile under O-poor conditions may play a role in the decreased photochemical activity of rutile as compared to anatase seen in experimental samples.

Acknowledgment. This research was supported by the Science Foundation Ireland under grant nos. 06/IN/1/I92 and 06/IN/1/I92/EC07. We also acknowledge support from the HEA for the PRTLI programs IITAC (cycle III). Calculations were performed on the IITAC supercomputer as maintained by the Trinity Centre for High Performance Computing (TCHPC), and the Stokes supercomputer, maintained by the Irish Centre for High-End Computing (ICHEC).

Supporting Information Available: Figures S1−S6 give geometries and interatomic distances for all defects. This material is available free of charge via the Internet at http://pubs.acs.org.

References and Notes

(1) Mills, A.; Elliott, N.; Hill, G.; Fallis, D.; Durrant, J. R.; Willis, R. L. *Photochem. Photobiol. Sci.* **2003**, *2*, 591.
(2) Fujishima, A.; Honda, K. *Nature* **1972**, *238*, 37&.
(3) O'Regan, B.; Grätzel, M. *Nature* **1991**, *353*, 737.
(4) Mattioli, G.; Filippone, F.; Alippi, P.; Amore Bonapasta, A. *Phys. Rev. B* **2008**, *78*, 241201(R).
(5) Henrich, V. E.; Cox, P. A. *The Surface Science of Metal Oxides*; Cambridge University Press: Cambridge, 1996.
(6) Henrich, V. E.; Kurtz, R. L. *Phys. Rev. B* **1981**, *23*, 6280.
(7) Aiura, Y.; Nishihara, Y.; Haruyama, Y.; Komeda, T.; Kodaira, S.; Sakisaka, Y.; Maruama, T.; Kato, H. *Phys. Rev. B: Condens. Matter* **1994**, *194−196*, 1215.
(8) Henrich, V. E.; Dresselhaus, G.; Zeiger, H. J. *Phys. Rev. Lett.* **1976**, *36*, 1335.
(9) Zhou, S.; Čižmar, A.; Potzger, K.; Krause, M.; Talut, G.; Helm, M.; Fassbender, J.; Zvyagin, S. A.; Wosnitza, J.; Schmidt, H. *Phys. Rev. B* **2009**, *79*, 113201.
(10) Yang, S.; Halliburton, L. E.; Manivannan, A.; Bunton, P. H.; Baker, D. B.; Klemm, M.; Horn, S.; Fujishima, A. *Appl. Phys. Lett.* **2009**, *94*, 162114.
(11) Nerlov, J.; Christensen, S. V.; Wichel, S.; Pedersen, E. H.; Moller, P. J. *Surf. Sci.* **1997**, *371*, 321.
(12) Khomenko, V. M.; Langer, K.; Rager, H.; Fett, A. *Phys. Chem. Miner.* **1998**, *25*, 338.
(13) Kurtz, R. L.; Stockbauer, R.; Madey, T. E. *Surf. Sci.* **1989**, *218*, 178.
(14) Nelson, J.; Chandler, R. E. *Coord. Chem. Rev.* **2004**, *248*, 1181.
(15) Cococcioni, M.; de Gironcoli, S. *Phys. Rev. B* **2005**, *71*, 035105.
(16) Mori-Sánchez, P.; Cohen, A. J.; Yang, W. *Phys. Rev. Lett.* **2008**, *100*, 146401.
(17) Morgan, J.; Scanlon, D. O.; Watson, G. W. *J. Surf. Sci. Nanotechnol.* **2009**, *7*, 389.
(18) Finazzi, E.; Di Valentin, C.; Pacchioni, G.; Selloni, A. *J. Chem. Phys.* **2008**, *129*, 154113.
(19) Na-Phattalung, S.; Smith, M. F.; Kim, K.; Du, M.-H.; Wei, S.-H.; Zhang, S. B.; Limpijumnong, S. *Phys. Rev. B* **2006**, *73*, 125205.
(20) Coquet, R.; Willock, D. J. *Phys. Chem. Chem. Phys.* **2005**, *7*, 3819.
(21) Scanlon, O.; Walsh, A.; Morgan, B. J.; Watson, G. W. *J. Phys. Chem. C* **2008**, *112*, 9903.
(22) Nolan, M.; Parker, S. C.; Watson, G. W. *Surf. Sci.* **2005**, *595*, 223.
(23) Scanlon, D. O.; Morgan, B. J.; Watson, G. W. *J. Chem. Phys.* **2009**, *131*, 124703.
(24) Scanlon, D. O.; Morgan, B. J.; Watson, G. W.; Walsh, A. *Phys. Rev. Lett.* **2009b**, *103*, 096405.
(25) Di Valentin, C.; Pacchioni, G.; Selloni, A. *Phys. Rev. Lett.* **2006**, *97*, 166803.
(26) Morgan, J.; Watson, G. W. *Surf. Sci.* **2007**, *601*, 5034.
(27) Calzado, J.; Hernández, N. C.; Sanz, J. F. *Phys. Rev. B* **2008**, *77*, 045118.
(28) Di Valentin, C.; Pacchioni, G.; Selloni, A. *J. Phys. Chem. C* **2009**, *113*, 20543.
(29) Morgan, B. J.; Scanlon, D. O.; Watson, G. W. *J. Mater. Chem.* **2009**, *19*, 5175.
(30) Di Valentin, C.; Pacchioni, G.; Onishi, H.; Kudo, A. *Chem. Phys. Lett.* **2008**, *469*, 166.
(31) Islam, M. M.; Bredow, T.; Gerson, A. *Phys. Rev. B* **2007**, *76*, 045217.
(32) Finazzi, E.; Di Valentin, C.; Pacchioni, G. *J. Phys. Chem. C* **2009**, *113*, 3382.
(33) Kresse, G.; Furthmuller, J. *Comput. Mater. Sci.* **1996**, *6*, 15.
(34) Kresse, G.; Furthmuller, J. *Phys. Rev. B* **1996**, *54*, 11169.
(35) Perdew, J. P.; Burke, K.; Ernzerhof, M. *Phys. Rev. Lett.* **1996**, *77*, 3865.
(36) Dudarev, S. L.; Botton, G. A.; Savrasov, S. Y.; Humphreys, C. J.; Sutton, A. P. *Phys. Rev. B* **1998**, *57*, 1505.
(37) Morgan, B. J.; Watson, G. W. *J. Phys. Chem. C* **2009**, *113*, 7322.
(38) Blöchl, P. E. *Phys. Rev. B* **1994**, *50*, 17953.
(39) Kresse, G.; Joubert, D. *Phys. Rev. B* **1999**, *59*, 1758.
(40) Yang, K.; Dai, Y.; Huang, B.; Feng, Y. 2009, arXiv:0910.5302v1.
(41) Zhang, C.; Michaelides, A.; King, D. A.; Jenkins, S. J. *Phys. Rev. B* **2009**, *79*, 075433.
(42) Keating, P. R. L.; Scanlon, D. O.; Watson, G. W. *J. Phys.: Condens. Matter* **2009**, *21*, 405502.
(43) Justicia, I.; Ordejón, P.; Canto, G.; Mozos, J. L.; Fraxedas, J.; Battiston, G. A.; Gerbasi, R.; Figueras, A. *Adv. Mater.* **2002**, *14*, 1399.
(44) Nazeeruddin, M. K.; Kay, A.; Rodico, I.; Humphry-Baker, R.; Müller; Liska, P.; Vlachopoulos, N.; Grätzel, M. *J. Am. Chem. Soc.* **1993**, *115*, 6382.
(45) Gajdos, M.; Hummer, K.; Kresse, G.; Furthmuller, J.; Bechstedt, F. *Phys. Rev. B* **2006**, *73*, 045112.
(46) Adolph, B.; Furthmuller, J.; Beckstedt, F. *Phys. Rev. B* **2001**, *63*, 125108.
(47) Yu, P. Y.; Cardona, M. *Fundamentals of Semiconductors*, 2nd ed.; Springer: New York, 1999.
(48) Ramos, L. E.; Paier, J.; Kresse, G.; Bechstedt, F. *Phys. Rev. B* **2008**, *78*, 195423.

(49) Paier, J.; Marsman, M.; Kresse, G. *Phys. Rev. B* **2008**, *78*, 121201.
(50) Kavan, L.; Grätzel, M.; Gilbert, S. E.; Klemenz, C.; Scheel, H. J. *J. Am. Chem. Soc.* **1996**, *118*, 6716.
(51) Elemental reference calculations consisted of a two-atom Ti cell with a 16 × 16 × 16 Γ-centered *k*-point mesh, at the zero-pressure identified by fitting to the Murnaghan equation of state, and a single triplet-state O_2 molecule placed at the center of a 15 × 15 × 15 Å cell, with only the Γ-point considered for *k*-point sampling.
(52) Lide, D. R., Ed. *CRC Handbook of Chemistry and Physics*, 79th ed.; CRC Press: New York, 1998.
(53) Reuter, K.; Scheffler, M. *Phys. Rev. B* **2002**, *65*, 035406.
(54) Finnis, W.; Lozovoi, A. Y.; Alavi, A. *Annu. Rev. Mater. Res.* **2005**, *35*, 167.
(55) Blumenthal, R. N.; Coburn, J.; Baukus, J.; Hirthe, W. M. *J. Phys. Chem. Solids* **1966**, *27*, 643.
(56) Deskins, A.; Dupuis, M. *Phys. Rev. B* **2007**, *75*, 195212.
(57) Deskins, A.; Rousseau, R.; Dupuis, M. *J. Phys. Chem. C* **2009**, *113*, 14583.
(58) Ganduglia-Pirovano, M.; Da Silva, J. L. F.; Sauer, J. *Phys. Rev. Lett.* **2009**, *102*, 026101.
(59) Migani, A.; Neyman, K. M.; Illas, F.; Bromley, S. T. *J. Chem. Phys.* **2009**, *131*, 064701.
(60) Lany, S.; Zunger, A. *Phys. Rev. B* **2008**, *78*, 235104.
(61) Janotti, A.; Van de Walle, C. G. *Phys. Rev. B* **2007**, *76,* 165202.
(62) Lany and Zunger [ref 60] have argued on symmetry grounds that localized defect states undergo little or no upward shift in energy when the position of extended states at the conduction band edge is extrapolated to experimental values. If this is valid for systems where the band edge and defect states can be constructed from equivalent atomic orbitals, the localized states described here have unchanged formation energies, whereas the partially delocalized state would be even more disfavored.
(63) Morgan, B. J.; Watson, G. W. *Phys. Rev. B* **2009**, *80*, 233102.

JP9088047